PROCEEDINGS, 51st Workshop on Geothermal Reservoir Engineering
Stanford University, Stanford, California, February 9-11, 2026
SGP-TR-230

Three dimensional Seismic Explorations in Kijiyama Geothermal Field in Akita, Japan Using the DFOS (Distributed Fiber Optic Sensing) System in Four Geothermal Boreholes in 2022, 2024, and 2025

Junzo Kasahara[1], Yoko Hasada, Masaru Suzuki, Tomohiro Takahashi, Hiroshi Ohnuma, Hisashi Tastunokuchi, Issei Higashi, Hiroki Saito, and Yu'ki Yamaura

1: Center for Integrated Research and Education of Natural Hazards, Shizuoka Univ., 836 Ohya, Surugaku, Shizuoka 422-8529, Japan

Kasahara.junzo@shizuoka.ac.jp

Keywords: Geothermal exploration, DAS, VSP, Seismic interferometry, *Vp/Vs*, S-to-P-conversion

ABSTRACT

In 2022, 2024, and 2025, we conducted a DFOS seismic study at the Kijiyam geothermal field in northeastern Japan. In 2022, we installed an optical fiber cable to depths of 2,000 m in the NS- and the EW-strike geothermal boreholes. We operated 25 vertical seismic sources around the Kijiyama geothermal plant under construction. In 2024, we also used the N-S and E-W horizontal vibrations at two stations. The DTS temperature was 294 °C at a depth of 2,000 m. Based on the DAS data obtained in 2022 and 2024 and synthetic seismic waveforms, we determined the 3D *Vp* depth distribution in this area. The extracted *Vp* profiles along five boreholes are compared with the borehole geology, and we confirm a reasonable fit. Migrated reflection shows intense reflections from 1 km to 4 km depth. We constructed a 3D composite diagram using *Vp* values, seismic reflection images, and locations of lost-circulation, flow-in, and flow-out along the well trajectories. We obtained anisotropy using the horizontal vibrations. The *Vp/Vs* for the N-S direction was approximately 2.0, in contrast to 1.95 for the E-W direction. This suggests the fracture diction is E-W direction down to 1,500m depth. In 2025, four new boreholes were drilled using our 3D *Vp* and reflection images. During the four well-drillings, we also conducted a new seismic survey in 2025, using two boreholes continuously for two months. During drilling at the S-W and E boreholes, we observed drill-bit noise by the N-S and vertical boreholes. We conducted a passive seismic study using the seismic interferometry technique, applying cross-correlation DAS data along NS and vertical boreholes. Combining all datasets in 2022, 2024, and 2025, we constructed the 3D *Vp* structure in the Kijima geothermal field. The challenge using the seismic interferometric technique using drill-bit noise and borehole DFOSs shows that it can be used for cross-hole seismic tomography. However, the quality of cross-correlated waveforms depends on the borehole situation and does not guarantee the performance of cross-hole tomography. We interpret the geothermal structure in the Kijiyama geothermal field using three years of datasets from 2022, 2024, and 2025.

1. INTRODUCTION

The use of supercritical water for geothermal energy is considered an enhanced geothermal system (EGS) due to its high enthalpy (Dobson *et al*., 2017; Friðleifsson *et al*., 2017; Reinsch *et al*., 2017). The critical point of pure water is 373.4 °C and 22.1 MPa. Pure water above this critical temperature and pressure is in a supercritical state, in which it exists between the liquid and gas phases. The location and nature of supercritical water reservoirs are yet to be well studied. One of the geothermal projects of the New Energy and Industrial Technology Development Organization (NEDO) focuses on identifying supercritical water reservoirs in Japan. One petrological hypothesis is that supercritical water is trapped beneath the silica cap rock (*e.g*., Amanda *et al*., 2022).

To develop a practical geophysical approach for investigating supercritical water, we conducted seismic exploration in geothermal fields in Japan (Kasahara *et al.*, 2019, 2020, 2022, 2025a-c). Because geothermal areas are covered by heterogeneous materials comprising volcanic sediments such as tuff, volcanic conglomerate, and altered andesites, it is difficult for seismic waves to penetrate the deeper zone beneath the surface layers. To reduce seismic-wave scattering from heterogeneous layers, we installed an optical fiber in a high-temperature geothermal borehole and used distributed temperature sensing (DTS) and distributed acoustic sensing (DAS). DAS technology has frequently been applied to VSP studies (*e.g*., Daley *et al*., 2013) and DAS studies have been used for geothermal applications (*e.g*., Chalari *et al*., 2019; Chang and Nakata, 2022; Feigl and Team, 2017; Feigl and Parker, 2019; Lellouch *et al*., 2021; Chen *et al*., 2022). We sought to determine the subsurface structure by acquiring seismic reflections from geothermal reservoirs, as fractures filled with fluid may generate strong reflections.

DTS and DAS technologies use Raman and Rayleigh backscattering of incident laser light in optical fiber, induced by strain or strain rate due to temperature changes and seismic-wave penetration, respectively (*e.g*., Hartog, 2017). Now it is called DFOS (Distributed Fiber Optic Sensing).

For our seismic study of a high-temperature geothermal field, we conducted geophysical exploration at the Kijiyama geothermal field

in northern Honshu, Japan, where plans are underway to construct a new geothermal power plant (Fig. 1).

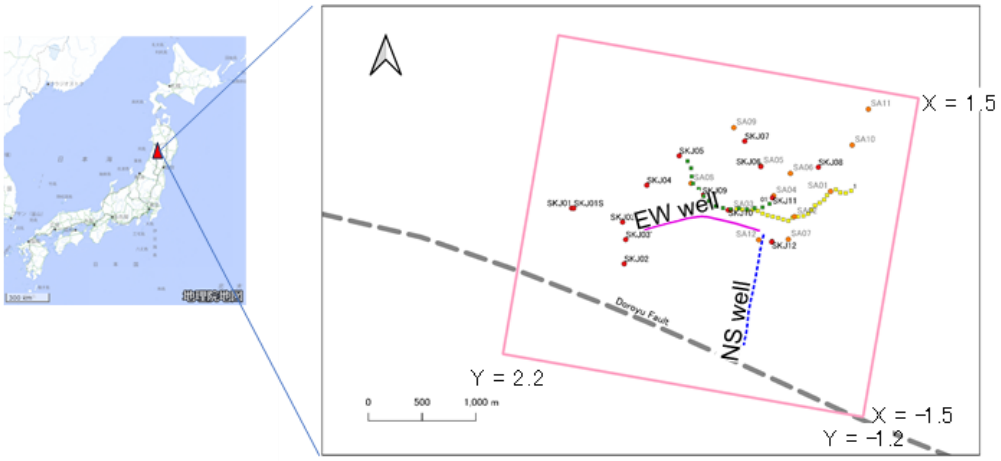

Figure 1: The location map of the Kijiyama survey in 2022 and 2024. For the data analysis, we used the EW and NS geothermal boreholes in 2024 and 2022, respectively. The 3D *Vp* distribution was obtained in the rectangular area.

2. GEOLOGICAL DESCRIPTION OF KIJIYAMA GEOTHERMAL FIELD

The Kijiyama geothermal field is located east of the Uenotai Geothermal Power Plant owned and operated by TOUSEC (Tohoku Sustainable and Renewable Energy Co., Ltd.). Quaternary volcanoes form finger-shaped lines perpendicular to the subduction trench axis (Tamura *et al.*, 2002). The Wasabibawa, Onikobe, and Uenotai geothermal power plants, located in a Quaternary volcanic region, are close to the Kijiyama geothermal field. Geothermal investigations in Uenotai and Kijiyama were conducted as part of the NEDO Minase survey NEDO, 1990) in which two boreholes, N63-MS-6 and N63-MS-8, were drilled in the Kijiyama geothermal field. The geological and geothermal model from Uenotai to Kijiyama was obtained by several drillings Naka and Okada, 1992; Futagoishi, 1999) (Fig. 2). We considered that the geological structure in Kijiyama was a continuation of the geological structure given by Nake and Okada (1992). According to the geological description in Fig. 2, the lithologies of Minasegwa and Doroyu are volcanic tuff and andesite, respectively. Detailed geological descriptions of the Doroyu formation in the Uenotai region are provided by Futagoishi (1999) , based on drilling data. The temperature at the bottom of the T43 borehole in the Uenotai region reached 335 °C (Naka and Okada, 1999).

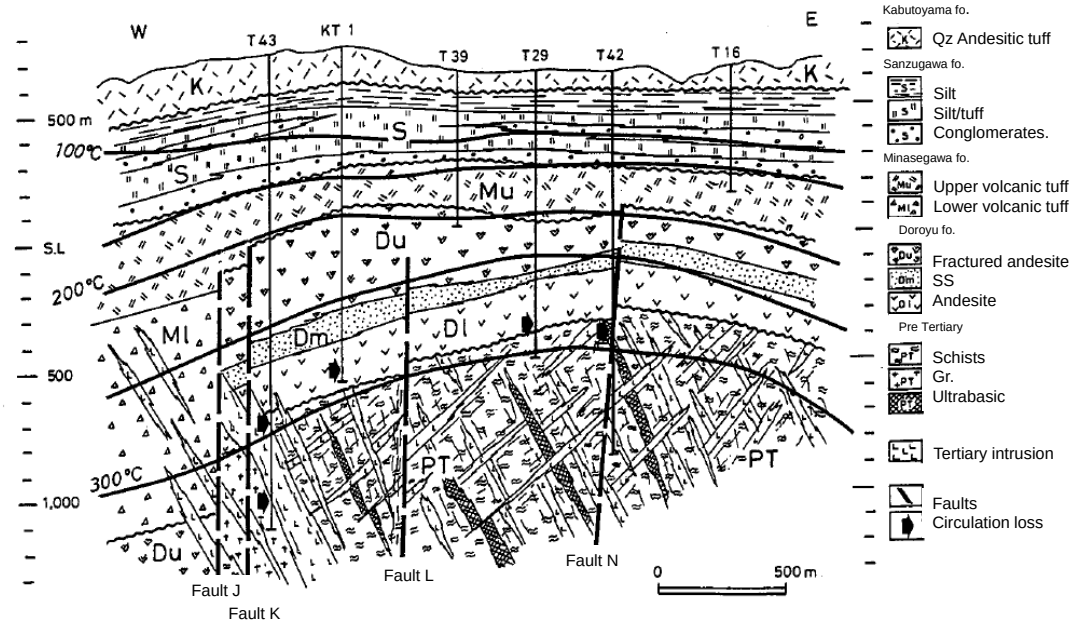

Figure 2: The E–W geological and geothermal model of Uenotai based on drilling data (Naka and Okada, 1992). T16 to T43 are boreholes. The T16 borehole is 800 m west of the N–S strike borehole in Kijiyama. The formations, from shallow to deep, are Sanzukawa (S), Minasegawa (Mu), Doroyu (Du), and the pre-Tertiary basement (PT).

Four other boreholes are near the NS borehole. The geological and geothermal sections of these five boreholes are available from TOUSEC (informal data), and we used this drilling information for the interpretation. The wellhead of the NS borehole is close to the 63-MS-6 and 63-MS-8 boreholes in the NEDO Minase project (NEDO, 1990). The NS borehole reaches a depth of 2,000 m (Fig. 1). The highest temperature for most of the boreholes in Kijiyama is close to 300 °C.

2. MEASUREMENT IN THE KIJIYAMA GEOTHERMAL FIELD

2.1 Field observation in 2022 and 2024

A single-mode optical fiber with a polyimide coating, housed in dual SUS tubes with N_2 circulation, was used in our study. We installed 2,000 m of optical fiber near the bottom of the NS borehole (Fig. 1). The DAS data were obtained using an ODH-4 interrogator unit with a 25 kHz ping rate, 1 ms sampling, and a 16.4 m gauge length. The DTS and DAS data were acquired at 1 m intervals along the fiber length. Twenty-six three-component seismometers were used at the ground surface along the E–W line (Fig. 1).

Twelve vertical seismic sources were excited north of the NS borehole wellhead in 2022, and another thirteen seismic sources were excited east of the E-W borehole in 2024 (in Fig. 1). EnviroVib was used for the vertical seismic source. One section of the vertical sweep was an upsweep from 10 to 75 Hz, lasting 30 s, followed by 30 s of sleep, with one-second cosine tapers at the beginning and end. One section of the horizontal sweep was 15 to 75 Hz during 30 s and 30 s of sleep. Each sweep was repeated approximately 500 times. We obtained the borehole temperature profile and seismic arrivals from active sources using DTS and DAS. We stacked the seismic data approximately 500 times using weighted stacking, accounting for DAS noise and surface seismic records, and removed the source signatures from the stacked data.

We obtained the 2D NS *Vp* depth profile by travel time tomography using the P first arrivals of the DAS and surface seismic data in2022 and 2024. Using a 2D *Vp* depth profile as the starting model, we obtained the 3D *Vp* structure from the first arrivals in DAS and surface seismometer records. We extracted the depth profile for each borehole from the 3D *Vp* structure and compared it with the borehole geology. We also compared our 3D *Vp* with the geological models made by TOUSEC.

The downgoing and upgoing phases in the DAS records were separated by applying a frequency–wavenumber (F-K) filter. The downgoing and upgoing phases corresponded to direct and reflected arrivals, respectively. We obtained reflection images by migrating upgoing phases corresponding to PP reflections.

We obtained a DAS record of the optical fiber's elongation induced by the shear source. Using the P- and S-wave arrivals in the shear excitation DAS records, we obtained the *Vp*/*Vs* ratio, thereby enabling estimation of fluid-filled fractures in the horizontal direction.

We observed numerous natural earthquakes and identified S-to-P conversions in DAS and surface seismometer records.

In this study, “well depth” was used for the length from the wellhead along the borehole, and “true depth” was used in the *Vp* structure, synthetic strain rate waveform calculation, and migration. We converted the well depth to true depth, accounting for the borehole's horizontal deviation.

2.2 Filed the operation in 2025

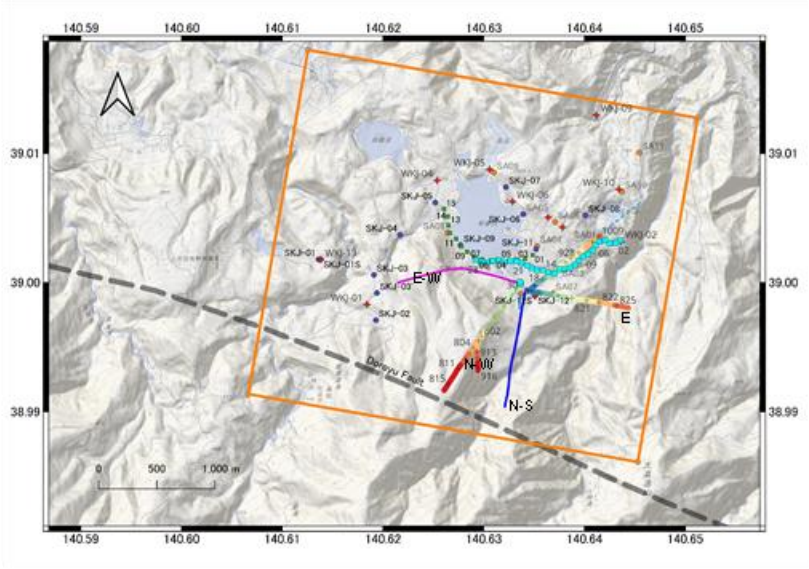

Figure 3: Location map of the 2025 experiment. The blue and purple lines are the NS and the EW boreholes. The red-yellow thick line shows the SW drilling borehole. The red to green thick line is the E drilling borehole. that squares are the locations of surface seismometers. All seismic vibrator locations in 2022,2024, and 2025 are shown by solid circles and solid stars. The thick, broken line is the Doroyu fault.

In 2025, we conducted a seismic interferometric study and active-source seismic exploration. In 2025, TOUSEC drilled four new boreholes in the Kijimaya geothermal field (Fig. 3). The SW is for the future production well, and the E borehole is for the future injection well. We used the vertical and NS boreholes for DAS observations via an independent optical fiber. For the active seismic source, we

used the HEMI 60 at 13 locations, each operated for 4 hours. We used two DAS interrogators: an ODH-4 from OptaSense and an IDAS from Silixa.

2.2.1 Passive seismic study by seismic interferometry technique using drill-bit noise

During the N and E borehole drillings, we observed drill-bit noise recorded by optical fibers in the NW and E boreholes. We performed cross-correlation using the DAS record at the reference depth, typically for 2 hours. We calculated the distance between the estimated drill-bit location at the specified time and optical fiber sensors, and generated the synthetic waveform using the previously obtained 3D Vp structure derived from the 2022 and 2024 datasets. We estimated the true travel time by minimizing the RMS error between the interferometric waveform and the synthetic travel time.

2.2.2 Vertical seismic source study

We used a 13 Hemi 60 seismic vibrator for 4 hours. The operational time sequence is identical to that in the EnviroVib case. For the 3D Vp structure study, we used interferometric data and an active source. Using the whole dataset from 2022, 2024, and 2025, we constructed a new 3D Vp structure and a PP migration image.

3. RESULTS

3.1 Results using the data of 2022 and 2024

The temperature profile of the EW borehole obtained by DTS measurement is shown in Fig. 4. The temperature was 294.3 °C at a well depth of 2058m. The temperature gradient shows an inflection at a well depth of 1.1 km, which may mark the lithological boundary between the Minasegawa and Doroyu formations.

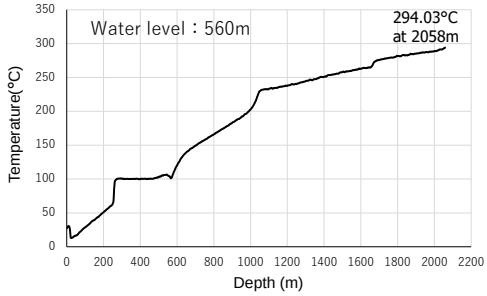

Figure 4: Temperature profile in the EW borehole of Kijiyama geothermal field. The depth is the length along the borehole. The water level is 560 m along the borehole.

The 0-offset DAS records at the SA-12 source, located near the wellhead of the N–S borehole, are shown in Fig. 5. The Vp gradient change with depth can be interpreted as the lithological boundary between the Minasegawa and Doroyu formations, based on a comparison of the geological description of the N–S borehole and the DAS records. However, the depth to the Vp lithological boundary is shallower than the depth of the change in the temperature gradient.

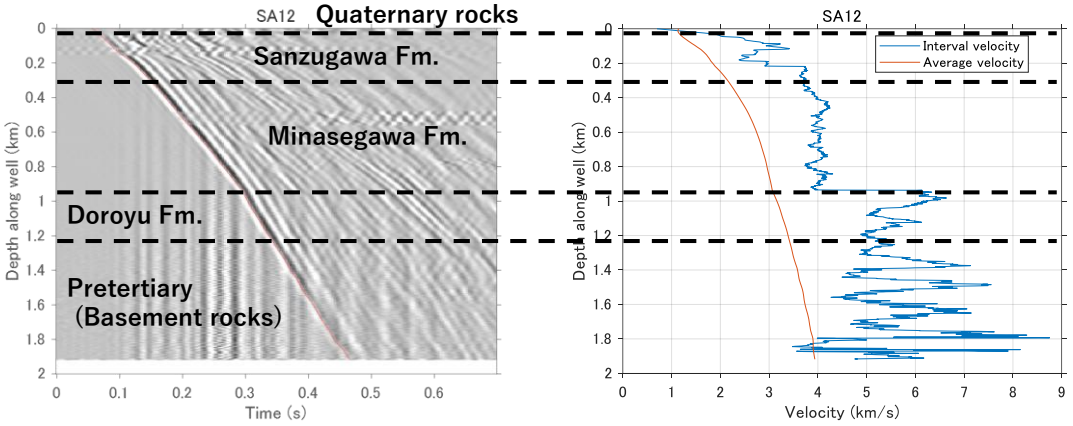

Figure 5: DAS record at SA-12 (left) and average *Vp* and interval *Vp* (right). The vertical axis is the well depth in kilometers along the borehole. The horizontal axes are the travel time in seconds and the *Vp* in kilometers per second, respectively. (Left) Lithological formations with average *Vp* values were interpreted by DAS records. (Right) Average *Vp* (red line) and interval *Vp* (blue line) with well depth. The lithological boundary was estimated using the geological description of the NS borehole drilling data (informal data from TOUSEC).

Fig. 6 shows DAS examples of 12 vertical and 1 horizontal seismic sources. The P first arrivals were observed in all DAS records obtained from vertical seismic sources. The S first arrivals were observed in the SH-01 DAS records obtained by the horizontal seismic source.

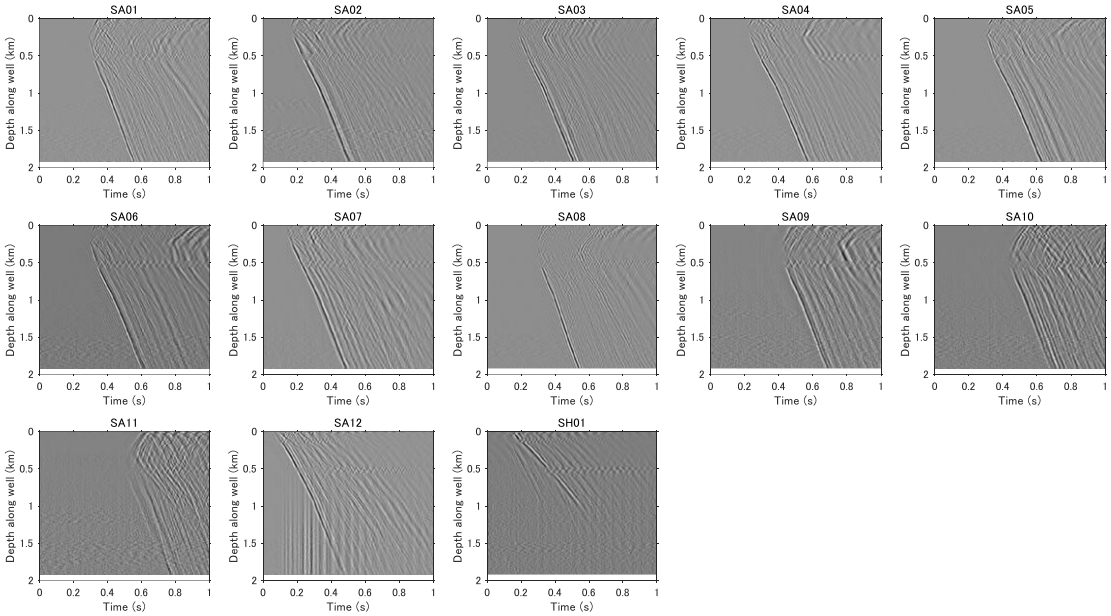

Figure 6: Twelve vertical DAS records (SA-01 to SA-12) and one horizontal DAS record (SH-01). Source locations are shown in Fig. 1. The vertical and horizontal axes denote well depth in kilometers along the borehole and travel time in seconds, respectively.

We obtained a 3D *Vp* structure from the P first arrivals recorded by the DAS and surface seismometers using 2022 and 2024. The *Vp* section along the NS and EW lines is shown in Fig. 7. According to the drilling data, the well depth of 970 m corresponds to the conglomerate–dacite tuff and altered andesite lithological boundary.

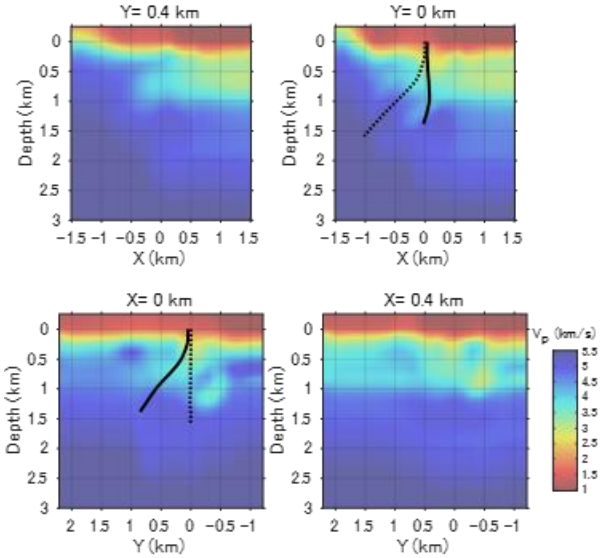

Figure 7: *Vp* depth profiles of near-NS (top two) and near-EW (bottom two). X and Y are shown in Fig. 1. Thick and broken lines are EW and NS borehole trajectories. The color shows *Vp* values.

The *Vp* structures corresponding to the geological and geothermal models of A-A′ to E-E (TOUSEC internal data) were extracted from the 3D *Vp* depth profile. One example in the case of A-A is shown in Fig. 8. The *Vp* structures resemble the geological and geothermal models. The Doroyu and pre-Tertiary layers correspond to a *Vp* zone with velocities exceeding 4 km/s. The thinning and thickening of the Minasegawa and Sanzugawa formations and Quaternary volcanics toward the south and north are identified in the *Vp* structure,

respectively. The other E–W geological models by TOUSEC (informal data) also show a similar *Vp* structure. The five 3D *Vp* structures corresponding to the five boreholes also resemble the borehole geology.

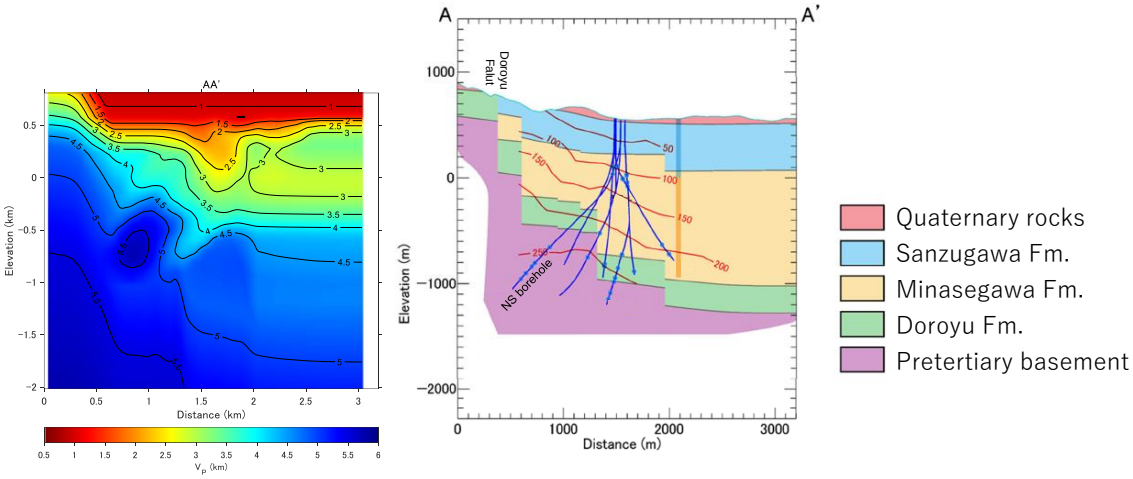

Figure 8: Comparison of the geological model A-A′ by TOUSEC (right, informal data) and the present *Vp* profile (left). The N–S borehole trajectories are indicated by the line on the left. The vertical axis is the true depth and the horizontal axis is the distance. The same area is shown.

We calculated the synthetic strain rate DAS waveforms in Fig. 9 sing the 3D *Vp* structure shown in Fig. 7 The observed P first arrivals (Fig. 9 satisfy the synthetic strain rate waveforms except for SA-1 due to the far distance from the borehole.

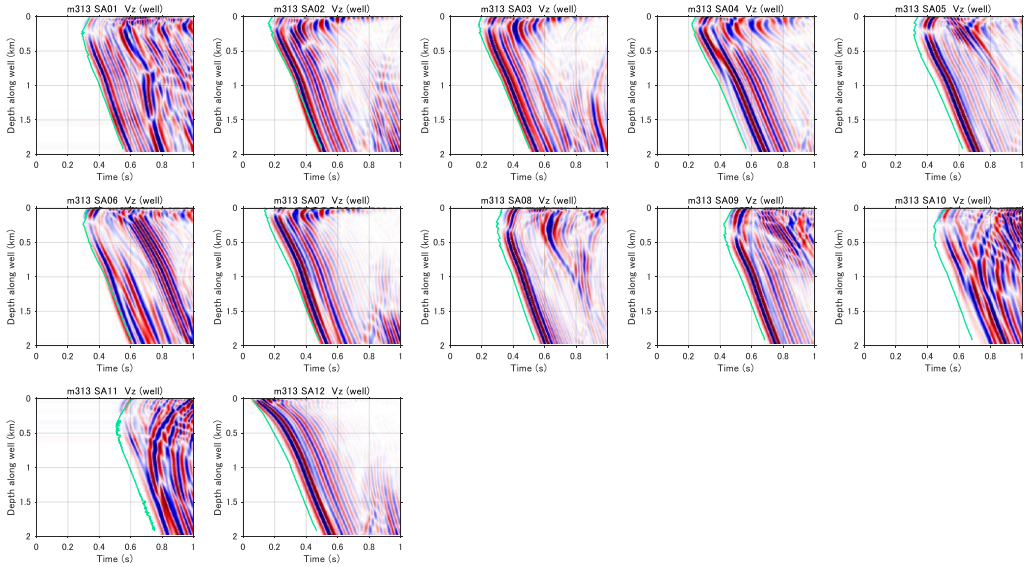

Figure 9: Synthetic strain rate DAS records of the twelve vertical seismic sources using the 3D *Vp* structure. The vertical and horizontal axes indicate well depth (kilometers) and travel time (seconds), respectively. The green line in each diagram indicates the observed P first arrivals.

Using the reflection data from the FK-filtered DAS records and the *Vp* structural model, we calculated the PP migration image (Fig. 10). The depth slices of the migration image are shown in Fig.10. The migration image identified intense reflectors at a true depth of 1.5–2 km. Deeper reflectors are also observed at true depths of 3–3.5 km and 4 km. The PP reflector near a true depth of 1 km corresponds to a change in the *Vp* gradient with depth, suggesting a lithological boundary. In particular, the high-intensity zones at depths of 2–2.5 km are more pronounced in the southwest region of the N–S borehole. A deep reflector around the depth of 3–4 km was identified west of the N–S borehole. The reflector at a depth of 0.6 km exhibits a weak intensity due to poor focusing.

We combined the 3D *Vp* depth profile and migration cross-section images (Fig. 11). Most reflectors deeper than 1.5 km are in the *Vp* > 5 km/s zone. The 3D expression of the migration image is shown in Fig. 12

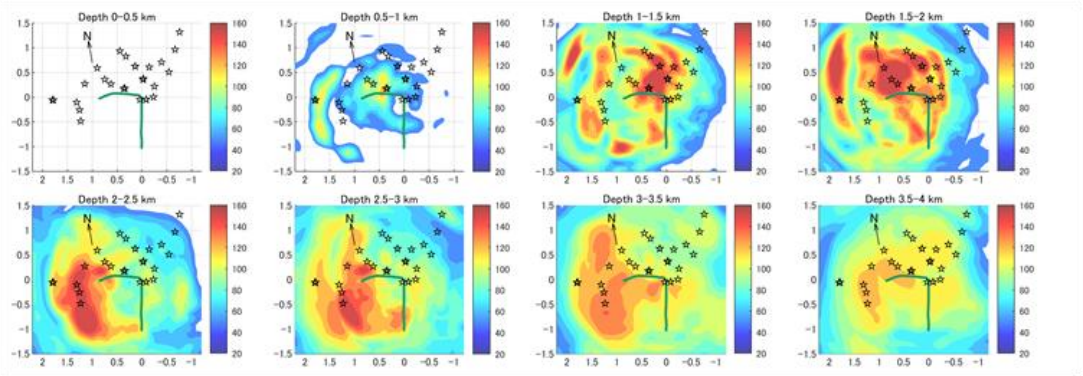

Figure 10: The depth slices of the migrated reflection image is shown. The red to blue colors denotes high to low intensity. The green lines show the trajectories of two boreholes. The stars are source locations for both surveys.

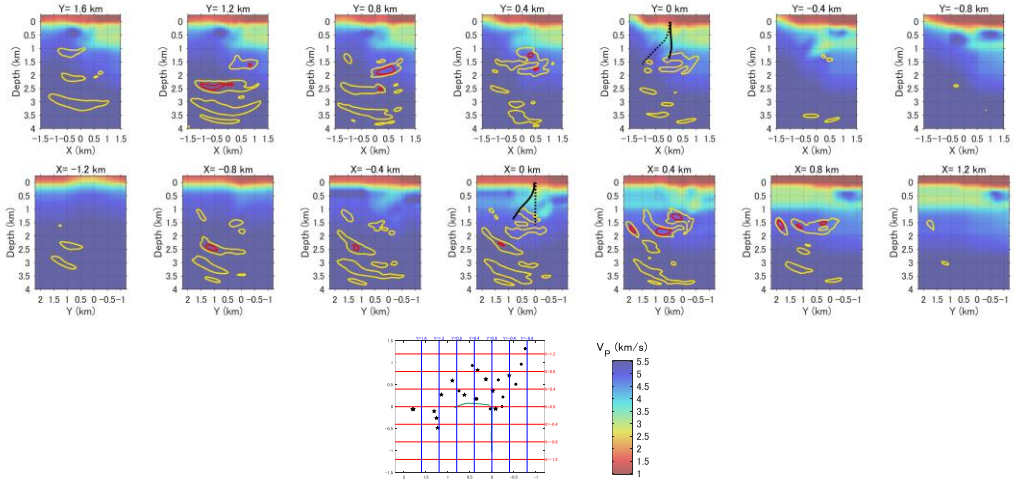

Figure 11: *Vp* depth profiles of near-NS (upper diagrams) and near-EW (lower diagrams). X and Y are shown in Fig. 1. Thick and broken lines are EW and NS borehole trajectories, respectively. The color scale for *Vp* is the same as in Fig. 3. The superposed red and yellow contour lines denote the reflection intensity.

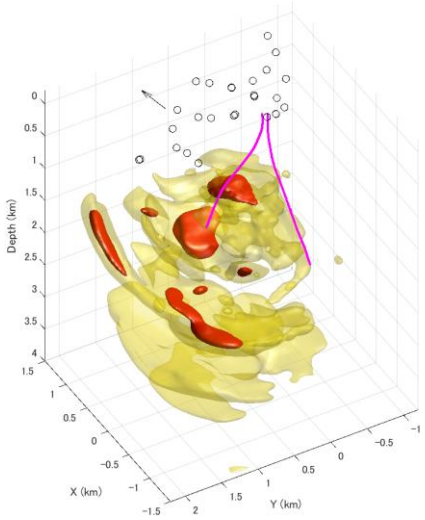

Figure 12: (Left) 3D migration image of PP reflections. The vertical axis is the true depth in kilometers. X-Y distances are the as in Fig. 6. The pink line indicates the trajectory of the N–S borehole. The borehole exhibits a horizontal deviation from a depth of 1 km. The 0 in the vertical axis is the elevation of the N–S borehole wellhead. Circles indicate the location of seismic sources. (Right) Cross sections at S10°W–N10°E and N80°W–S80°E of the 3D migration image. Stars indicate seismic sources. High to low intensities are shown on a color scale.

3.2 Results of horizontal vibrations

From the horizontal vibrations at SA01 and SA-12, we obtained S arrivals on the DAS records for the NS and EW components (Fig. 13).

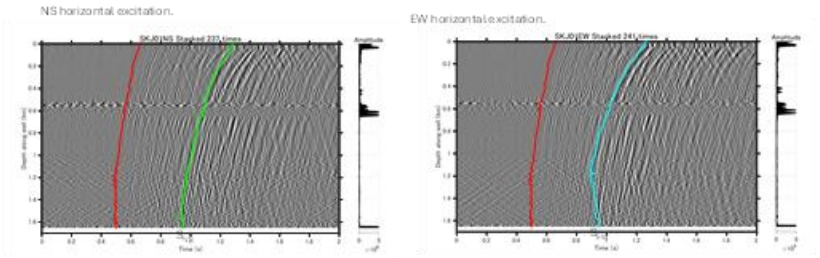

Figure 13: Tree DAS records of vertical, NS, and EW horizontal vibrations by the optical fiber in the EW borehole. The vertical axis is the length along the fiber. The horizontal axis is the elapsed time in seconds. The red line, green, and blue lines indicate the P, SNS, and S_{EW} arrivals.

We picked the P and S_{NS} and S_{EW} arrivals and calculated Vp-V_{s_NS} and Vp/V_{s_EW} (Fig.14). The Vp/Vs for the NS vibration is larger than Vs for EW vibration. This suggests anisotropy due to fractures aligned in the EW direction. The anisotropy of schist was measured by the ultrasonic method, and the results show Vp, $Vs//$ and $Vs\perp$ along the schistosity are 6.0 km/s, 3.5km/s and 2.8 km/s, respectively (Kasahara *et al*., 1968). On the other Vp, $Vs\perp$ *and* $Vs//$ are 3.4 km/s, 2.7km/s and 2.7 km/s. The corresponding Vp/Vs for the parallel and perpendicular directions along the schistosity are 1.71 and 2.14, respectively. The shear measurement in the Kijiyama geothermal field, Vp/V_S for NS=1.95 and 1.8 for EW. Therefore, we think the lower Vp/Vs for the EW direction is similar to the schistosity, which is the direction of fracture

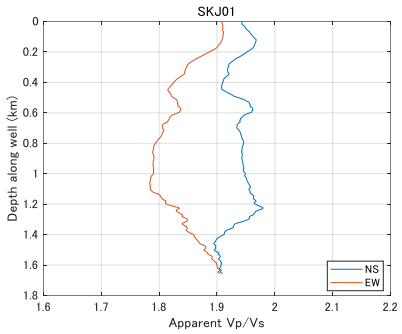

Figure 14: *Vp/Vs* depth profile obtained by the EW and NS horizontal vibrations and the DAS data in the EW borehole. The *Vp/Vs* for the NS vibrations show larger *Vp/Vs* for the EW vibration.

3.3 S to P conversion seen in natural earthquake records

We observed numerous earthquakes during the two-week study. One of the earthquake records is shown in Fig. 15. We identified clear P first arrivals in the DAS records and the UD components of the surface seismometers. The N–S and E–W seismometer components showed S arrivals, but the UP components corresponding to the S parts showed S arrivals approximately 0.25 s earlier than the N–S and E–W components. DAS records showed three arrival groups with velocity Vp immediately preceding the S arrivals. These arrivals are considered as S-to-P conversion at well depths of 2.0, 1.0, and 0.6 km. The surface seismic records show S-to-P conversion arrivals at well depths of 2.0, 1.0, and 0.6 km.

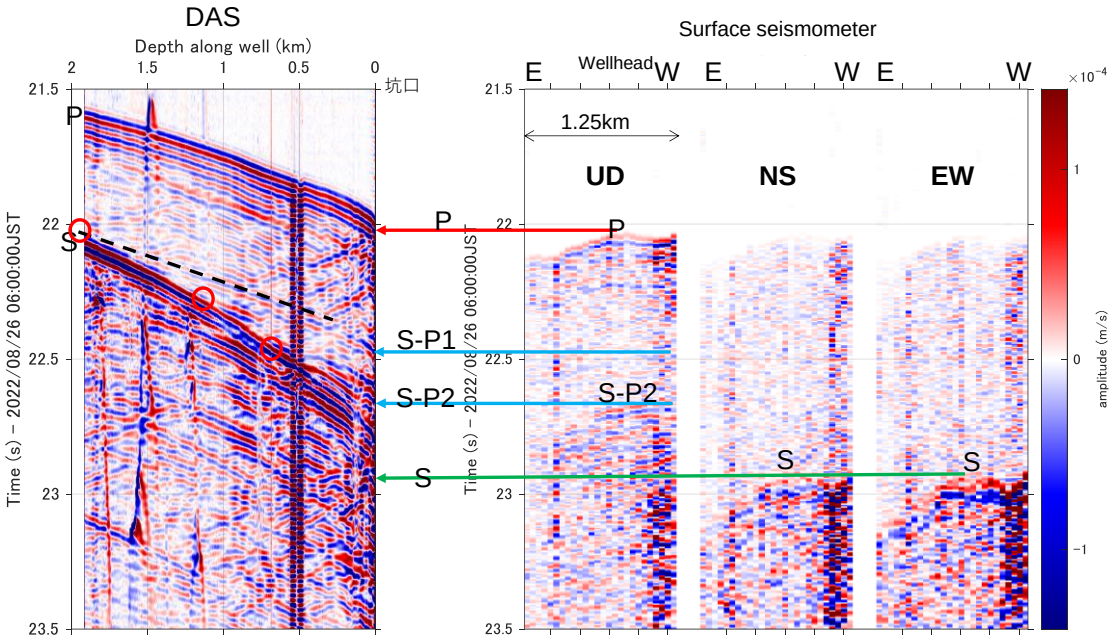

Figure 15: S-to-P conversion seen in DAS (right) and three-component surface seismic records for DAS (left) and three-component seismometer (right) records of a natural earthquake in Akita prefecture, which occurred at 06:00:20.7 JST on August 26, 2022 (M = 0.7, depth = 3 km). Three S-to-P conversion phases at a depth of 2.0, 1.0, and 0.6 km were identified by DAS and surface seismometers.

3.4 Results including the seismic data obtained in 2025

During the drillings of new boreholes, we recorded noise from drill-bits. By the cross-correlation of waveforms along the N-S and

The waveforms were obtained by cross-correlating DAS waveforms along the borehole at a reference depth. Two examples are shown in Fig. 15. We can identify arrivals from drilling bit noise at the E and N-W boreholes.

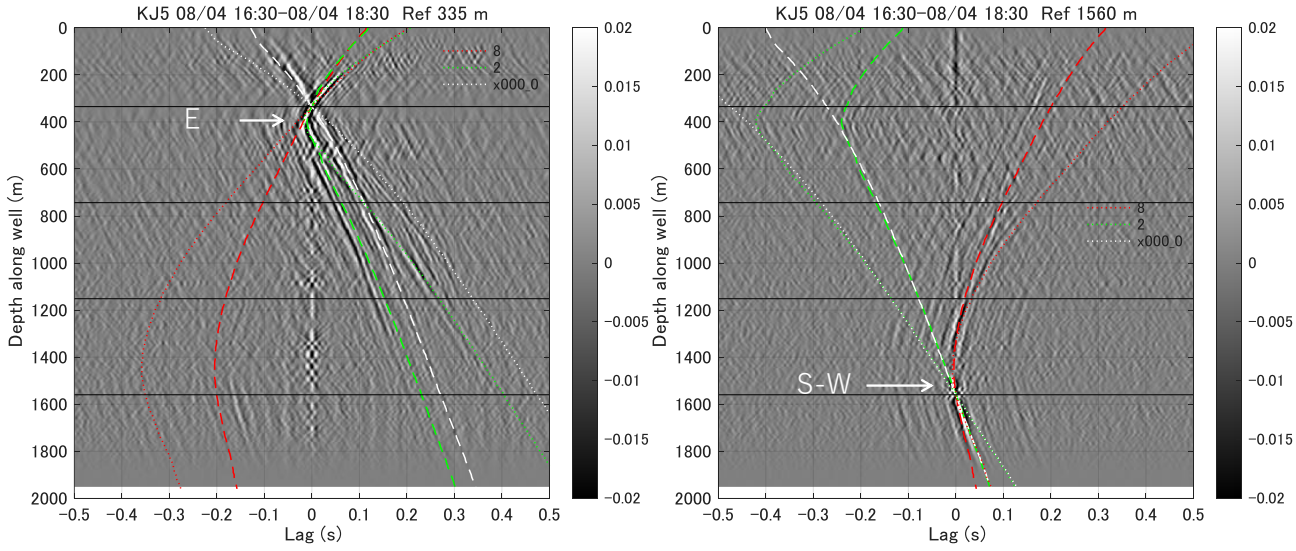

Fig. 16: (Left) Cross-correlations with the reference depth of 335m. (Right) Cross-correlation with the reference depth of 1560m.

Including the cross-correlation arrivals and 38 active sources in 2022, 2024, and 2025, we obtained a new 3D Vp structure (Fig. 17). The comparison of the previous Vp model (model 328) and the new result (Model 330) is shown in Fig. 18. The difference is not so large, but there are some changes at deeper part.

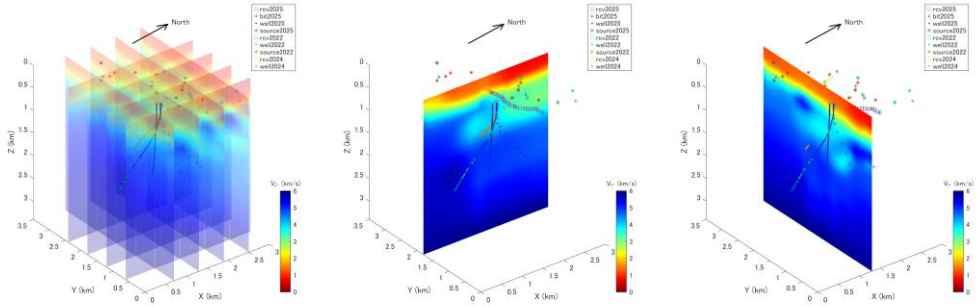

Fig. 17: The Vp 3D distribution obtained using the whole dataset in 2022, 204, and 2025. (Left) 3D view of the new Vp structure. (Middle)Vp depth section of the NS line. (Right) Vp depth section of the EW line

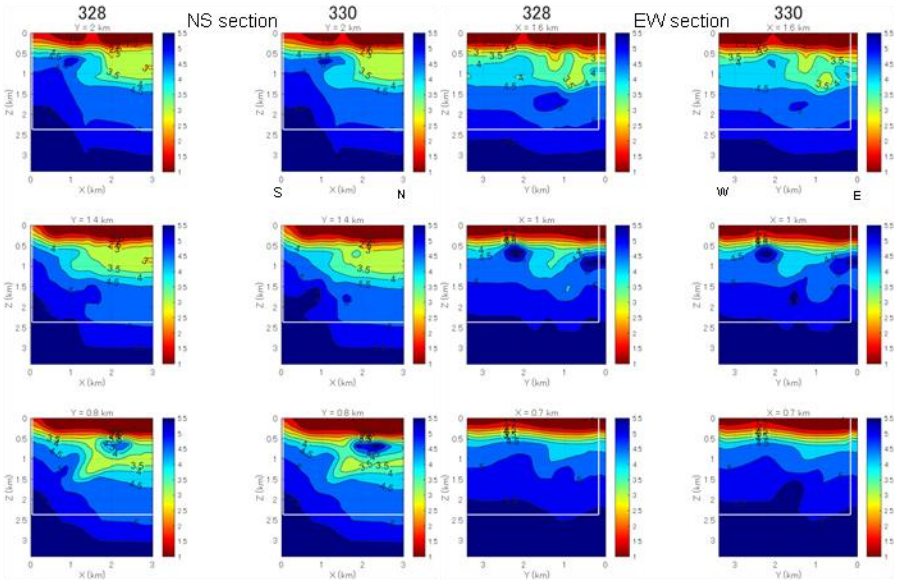

Fig. 18: Comparison of Vp depth cross-section in the previous study (model 328) and the new joint study (model 330).

4. DISCUSSION AND CONCLUSIONS

In 2022 and 2024, we conducted geothermal seismic exploration using active seismic sources and two borehole DFOS. We obtained the 3D Vp structure and the reflection image using the DFOS data and surface seismometer array. In 2025, we obtained a new dataset during the new borehole drillings. Using the seismic interferometry technique, we obtained a cross-hole seismic dataset. In addition, we conducted 31 active seismic source exploration projects. Using the whole dataset, we constructed a new Vp structure. The new result shows improvement in the deeper part.

We added new subsurface information in developing a geothermal field using DAS and DTS measurements in one hot geothermal borehole and seismic excitations. Fluid zones in the geothermal field could have generated these seismic reflections. The intense PP reflector at approximately 0.97 km marks the lithological boundary between the Minasegawa and Doroyu formations, where *Vp* values change from approximately 3.5 to 5 km/s. The seismic reflectors at true depths of around 2–2.5 km and 4 km in the migration image could imply unknown geothermal reservoirs. The reflection at a true depth of approximately 4 km may indicate a supercritical water reservoir, because the critical point of pure water is 374 °C and 22.1 MPa, and the temperature at the N–S borehole was 288 °C at a well depth of 2 km.

Using shear vibration, we obtained SH arrivals at a well depth of 1,200 m. Using P and S arrivals and an estimated origin time, we obtained *Vp/Vsh* = 1.75, approximately the same as that of ordinary rocks. S waves vibrating perpendicular and parallel to the geothermal fractures filled with fluid show slower and ordinary V_S velocities, suggesting the absence of dominant horizontal fracturing. According to

their measurements of schist rock (Kasahara *et al*., 1968) showed V_P, V_{S1}, V_{S2} = 6.0, 3.5, 2.7 km/s for traveling in the X direction parallel to the schistosity and V_P, V_{S1}, V_{S2} = 3.5, 2.7, and 2.75km/s for traveling in the Z direction perpendicular to the schistosity. Using these numbers, *Vp/Vs* = 1.72, 2.22 for the X direction, and 1.29 for the Z direction. The shear measurement in the Kijiyama geothermal field, *Vp/Vs* for NS=1.95and 1.8 for EW. Therefore, we think the lower *Vp/V*s for the EW direction is similar to the schistosity that is the direction of fracture.

We identified the S-to-P conversions of a natural earthquake at well depths of 0.6, 1.0, and 2.0 km. These conversion depths correspond to *Vp*, temperature, lithological boundaries, and seismic reflection zones.

The challenge using the seismic interferometric technique using drill-bit noise and borehole DFOSs shows that it can be used for cross-hole seismic tomography. However, the quality of cross-correlated waveforms depends on the borehole situation and does not guarantee the performance of cross-hole tomography.

ACKNOWLEDGMENTS

This paper is based on results from the New Energy and Industrial Technology Development Organization (NEDO JPNS21991 and JPNP21001) sincerely thank the officers at NEDO for their continuous support during our studies. We also sincerely thank Tohoku Sustainable and Renewable Energy (TOUSEC) Co., Ltd. for granting permission to use their geothermal borehole and for providing their informal database of geothermal fields. We also thank Welma Co., Ltd., Hanshin Consultants Co., Ltd., and Daiwa Exploration and Consulting Co., Ltd. for their assistance with fieldwork.

REFERENCES

Amanda, F. F., Tsuchiya, N., Alviani, V., Uno, M., Yamada, R., Shimizu, S., Oyanagi, R. High-temperature silicified zones as potential caprocks of supercritical geothermal reservoirs, Geothermics, (2022) https://doi.org/10.1016/j.geothermics.2022.102475.

Cheng, F., Ajo-Franklin, J.B., Nayak, A., Tribaldos, V. R., Mellors, R., Dobson, P., and the Imperial Valley Dark Fiber Team, (2022) Using Dark Fiber and Distributed Acoustic Sensing to Characterize a Geothermal System in the Imperial Valley, Southern California, JGR Solid Earth, 10.1029/2022JB025240.

Chalari, A., Mondanos, M., Coleman, T., Farhadiroushan, M., and Stork, A. Seismic methods for geothermal reservoir characterization and monitoring using fiber optic distributed acoustic and temperature sensor. In EAGE/BVG/FKPE Joint Workshop on Borehole Geophysics and Geothermal Energy (Vol. 2019, pp. 1–6)(2019) .

Chang, H., and Nakata, N. Investigation of time-lapse changes with DAS borehole data at the Brady geothermal field using deconvolution interferometry. Remote Sensing, 14(1), (2022) 185. https://doi.org/10.3390/rs14010185.

Daley, T. M., Freifeld, B. M., Ajo-Franklin, J., Dou, S., Pevzner, R., Shulakova, V., et al. (2013) Field testing of fiber-optic distributed acoustic sensing (DAS) for subsurface seismic monitoring. The Leading Edge, 32(6),699–706. https://doi.org/10.1190/tle32060699.1

Dobson, P., Asanuma, H., Huenges, E., Poletto, F., Reinsch, T., and Sanjuan, B. (2017). Supercritical geothermal system – A review of past studies and ongoing research activities, Proceedings of 41st Workshop on Geothermal Reservoir Eng., Stanford Univ., Stanford, California, Feb. 13–15.

Feigl, K. L., and Parker, L. M. (2019) Porotomo final technical report: Poroelastic tomography by adjoint inverse modeling of data from seismology, geodesy, and hydrology (Technical Report). University of Wisconsin. https://doi.org/10.2172/1499141.

Feigl, K. L., and Team, P. (2017) Overview and preliminary results from the PoroTomo project at Brady Hot Springs, Nevada: Poroelastic tomography by adjoint inverse modeling of data from seismology, geodesy, and hydrology. In a paper presented at the 42nd Workshop on Geothermal Reservoir Engineering (pp. 1–15).

Friðleifsson, G. O., Elders, W. A., Zierenberg, R. A., A., Fánsson, A., Fowler, P. G., Weisenberger, T. B., Harðarson, B. S., and Mesfin, K. G. (2017). The Iceland Deep Drilling Project 4.5 km deep well, IDDP-2, in the seawater-recharged Reykjanes geothermal field in SW Iceland has successfully reached its supercritical target, Sci. Drill., 23, 1–12, https://doi.org/10.5194/sd-23-1-2017.

Futagoishi, M. (1999) The Uenotai Geothermal Field – From Investigation and Development to Recent Operation, Journal of the Geothermal Research Society of Japan, Vol. 21, No. 3, 225–235.

Hartog, A. H. (2017) An introduction to distributed optical fiber sensors, RC Press. 440 pp.

Kasahara, J., Kumazawa, M., and Iida, K. (1968) Plane and Spherical Wave Velocities and Energy Flow in Anisotropic Media, Jour. Seismol. Soc. Japan, 21, 282–292.

Kasahara, J., Hasada, Y., Kuzume, H., Fujise, Y., and Yamaguchi, Y. (2019) Seismic feasibility study to identify supercritical geothermal reservoirs in a geothermal borehole using DTS and DAS, EAGE extended abstract, EAGE 2019 Annual Meeting, London.

Kasahara, J., Hasada, Y., Kuzume, H., Mikada, H., and Fujise, Y. (2020) The second seismic study at the geothermal field in southern Kyushu, Japan using an optical fiber system and surface geophones, Proceedings of 44th Workshop on Geothermal Reservoir Engineering, Stanford University, Stanford, CA.

Kasahara, J., Hasada, Y., Kuzuma, H., Ohnuma, H., Mikada, H., and Fujise, Y. (2022) A field experiment of a temperature-tolerant distributed acoustic sensor in deep geothermal reservoir prospecting, The Leading Edge, May, (2022)331–337.

Kasahara, J., Hasada, Y., Furuya, S., Shimazaki, M., Ohnuma, H., Mikada, H., and Fujise, Y. (2025a) DAS and DTS geophysical study in the Takigami geothermal field in northeastern Kyushu, Japan, in "Distributed Acoustic Sensing in Borehole Geophysics," AGU Monograph, Wiley Pub.

Kasahara, J., Hasada, Y., Ohnuma, H., Mikada H., and Fujise, Y. (2025b) Geothermal study using optical fiber sensing method in geothermal boreholes at Sumikawa, Japan, in "Active Geophysical Monitoring," 3rd edition, edited by Mikada, Zhdanvov and Kasahara, Elsevier Pub.

Kasahara, J., Hasada, Y., Kuzume, H., Mikada, H., and Fujise, Y. (2025c) Geophysical exploration at Ohnuma geothermal area using optical fiber system, "Active Geophysical Monitoring," 3rd edition, edited by Mikada, Zhdanov and Kasahara, Elsevier Pub.

Lellouch, A., Schultz, R., Lindsey, N. J., Biondi, B., and Ellsworth, W. L. (2021) Low-magnitude seismicity with a downhole distributed acoustic sensing array – Examples from the forge geothermal experiment. Journal of Geophysical Research: Solid Earth, 126(1), e2020JB020462. https://doi.org/10.1029/2020jb020462.

Naka, T., and Okada, H. (1992) Exploration and development of Uenotai geothermal field, Akita prefecture, northeastern Japan, Mining Geology, 42(4), (1992) 223–240.

New Energy Industrial Technology Development Organization (NEDO) (1990) Geothermal Development Promotion Survey Report of Minase Area, No. 20, 1281pp., (in Japanese).

Reinsch, T., Dobson, P., Asanuma, H., Huenges, E., Poletto, F., and B. Sanjuan, B. (2017) Utilizing supercritical geothermal systems: a review of past ventures and ongoing research activities, Geothermal Energy, https://doi.org/10.1186/s40517-017-0075-y, 5, Article number: 16.

Tamura, Y., Tatsumi, Y., Zhao, D., Kido, Y., and Shukuno, H. (2002) Hot fingers in the mantle wedge: new insights into magma genesis in subduction zones. Earth and Planetary Science Letters 197, 105–116. https://doi.org/10.1016/S0012-821X(02)00465-X.